Experimental investigation on the behaviour of FRP strengthened square hollow section (SHS) steel members under monotonic and cyclic loading

T. Tafsirojjaman [a,b*], Nicholas Wirth [b], David P Thambiratnam [b], N.H. Ramli Sulong [b], Allan Manalo [c], Sabrina Fawzia [b]

[a] School of Architecture and Civil Engineering, The University of Adelaide, Adelaide 5005, Australia;

[b] School of Civil and Environmental Engineering, Faculty of Science and Engineering, Queensland University of Technology, 2 George Street, Brisbane, QLD 4000, Australia.

[c] Centre for Future Materials (CFM), School of Civil Engineering and Surveying, University of Southern Queensland, Toowoomba, QLD, 4350, Australia.

(*Corresponding author: tafsirojjaman@adelaide.edu.au, Tel: +61883130828)

Experimental investigation on the behaviour of FRP-strengthened SHS steel members under monotonic and cyclic loading

ABSTRACT

Strengthening and rehabilitation of square hollow sections (SHS) is a major concern nowadays as SHS may fail due to higher service loads, fabrication and construction errors, degradation of material over time and adverse effects of the cyclic loading due to earthquakes. In the present study, a detailed experimental investigation has been carried out for the implications of using CFRP and GFRP as a strengthening measure to mitigate the failure of SHS members under monotonic and cyclic loadings. Strengthened members displayed lower moment degradation and higher moment and energy dissipation capacities and higher stiffness and ductility compared to the bare steel members. Although the amount of CFRP and GFRP fibres were almost equal, CFRP strengthening can result in higher capacity sections due to having higher strength material properties compared to GFRP strengthening. The cyclic responses of the GFRP-strengthened member were close to that of the CFRP-strengthened member and can be more effective for strengthening steel SHS under cyclic flexural loading. The established theoretical model in the current paper can predict reliably the ultimate moment capacities of the strengthened SHS members. This study confirmed that strengthening SHS members with fibre composites will be effective for structures in seismically active regions.

KEYWORDS

Steel SHS member; Structural performances; Monotonic loading; Cyclic flexural loading; CFRP; GFRP; Strengthening; Prediction model.

1. Introduction

Structures in seismically active regions must be designed for cyclic loading along with the live and dead loads. Earthquakes can often lead to failures and casualties and be responsible for taking more than 1.87 million lives in the 20th century (Guha-Sapir et al., 2015). On average, every earthquake is causing 2052 deaths between 1990 and 2010 (Guha-Sapir et al., 2015), and the rate of earthquake occurrence has been increasing (Nazri, 2015). This increase in seismic activity leads to a greater need to understand the effects of earthquakes on different infrastructure systems including steel frame buildings (ANSI/AISC 341-16, 2016; Seica & Packer, 2007).

The design of steel structures in seismic and cyclic loading regions requires careful consideration. These structures can fail through the cracking or fracture of critical members (Domaneschi, 2012; Martinelli & Domaneschi, 2017). The Northridge earthquake in 1994 caused massive damage to healthcare and numerous other steel-framed structures, both old and new, low-rise and high-rise. Cracks occurred in the structural steel members. Moreover, plastic hinges were formed which were overloaded further and led to failure (Charalampakis et al., 2019). Moreover, seismic loading can cause failures in the structural members and connections of the structures or the entire collapse of the structures (Kaan et al., 2012). Fadden and McCormick (Fadden & McCormick, 2011) conducted an experimental investigation on the structural performance and failure modes of steel hollow beam members (square and rectangular hollow sections) under quasi-static large displacement cyclic bending loading. Hollow cantilever beam members failed due to local buckling and fracture in the flange at the support end. Azevedo and Calado (Azevedo & Calado, 1994) evaluated the hysteretic behaviour of steel beam members (I-section). The members failed due to the buckling of the flange and web at the support ends. Therefore, effective methods of strengthening the steel

elements subject to cyclic loading should be determined to minimise or eliminate their adverse effects on infrastructure.

Fibre reinforced polymers (FRP) are become very popular to repair and strengthen civil infrastructures (M. I. Alam et al., 2017; Kadhim et al., 2018; Liu et al., 2020, 2021, 2022; Manalo et al., 2016; Mohammed et al., 2020; Tafsirojjaman, Fawzia, & Thambiratnam, 2020a; Zhao & Zhang, 2007) because of many advantageous characteristics of FRPs. For instance, the advantageous characteristics of FRPs are lightweight (Batuwitage et al., 2017; Gao et al., 2013), high corrosion resistance (Tafsirojjaman, Fawzia, & Thambiratnam, 2019b; Tafsirojjaman, Fawzia, Thambiratnam, & Wirth, 2021), high tensile strength (Tafsirojjaman, Fawzia, & Thambiratnam, 2021; Tafsirojjaman, Fawzia, Thambiratnam, et al., 2020a), design and installation flexibility (Tafsirojjaman, Fawzia, Thambiratnam, et al., 2020b) and require less labour during preparation and installation (Tafsirojjaman, Fawzia, & Thambiratnam, 2020b). Many studies have shown that carbon fibre reinforced polymer (CFRP) wrapping is an effective method of increasing the structural capacity of square and rectangular hollow sections (SHS and RHS, respectively) under static loading (Keykha, 2019; Photiou et al., 2006; Zhao et al., 2006). These studies have also highlighted that CFRP-strengthened RHS has increased load and moment capacities over bare steel sections under static loading. The ductility of strengthened RHS members can increase under bending and axial loadings (Photiou et al., 2006; Zhao et al., 2006). Local and torsional buckling can also be delayed in retrofitted steel members tested compared to the steel alone (Keykha, 2019; Photiou et al., 2006; Zhao et al., 2006) as the FRP increases the thickness of FRP which reduces the slenderness as well as enhances the stiffness. Moreover, Manalo et al. (Manalo et al., 2016) demonstrated that the prepreg FRP repair method can reinstate the original load capacity and stiffness of steel I-sections with pretended defects on the tension flange subjected to bending. The load capacity and stiffness were increased in the universal I-beam (UB) and circular hollow section (CHS)

beams when strengthened by CFRP under bending due to delaying buckling (Siwowski & Siwowska, 2018; Tafsirojjaman, Fawzia, Thambiratnam, et al., 2019a). In addition, the CFRP strengthening enhanced the moment and dissipated energy capacity and ductility of CHS members under cyclic loading as CFRP strengthening increased the rotational capacity of the members (Tafsirojjaman, Fawzia, Thambiratnam, et al., 2019a). Moreover, CFRP strengthening can enhance the durability of steel members effectively (Kabir, Fawzia, & Chan, 2016; Kabir, Fawzia, Chan, & Gamage, 2016).

The glass fibre reinforced polymer (GFRP) strengthening technique has enhanced the structural performance of steel UB and CHS beams under static as well as cyclic flexural loading (Accord & Earls, 2006; El Damatty et al., 2003; Harries et al., 2009; Photiou et al., 2006; Siddique & El Damatty, 2013). Local buckling of flanges was reduced in the GFRP-strengthened RHS, SHS and UB sections (Accord & Earls, 2006; El Damatty et al., 2003; Harries et al., 2009; Photiou et al., 2006; Siddique & El Damatty, 2013). These research studies showed the high possibility of strengthening structural steel members with either CFRP or GFRP composites. Typically, SHS is popularly used in civil infrastructures as columns, bracing members, and structural elements in truss and cladding supports due to the exceptional bending, compression and torsional behaviours of SHS. The vulnerable effects of cyclic loading on SHS members during earthquakes are a major concern. However, the effectiveness of the strengthening of steel SHS members with CFRP and GFRP composites to improve the cyclic or seismic performances of steel SHS beams has yet not been evaluated in detail.

CFRP and GFRP strengthening methods can effectively mitigate the vulnerable effect of cyclic or seismic loading on CHS steel members under monotonic and cyclic loading (Tafsirojjaman, Fawzia, Thambiratnam, & Wirth, 2021). However, there is limited investigation reported in the literature on FRP-strengthened SHS members under bending (Photiou et al., 2006). Moreover, structural rehabilitation of existing SHS members by

strengthening with CFRP and GFRP to mitigate the vulnerable effect of cyclic or seismic loading on simply-supported steel SHS members has yet not been investigated in the literature. Therefore, a detailed experimental investigation has been conducted on the behaviour of the simply supported SHS members strengthened with CFRP and GFRP subjected to three-point monotonic and cyclic flexural loading in the current study. The structural responses and failure modes under static and cyclic loadings of the bare and strengthened members are comparatively evaluated for the implications of using CFRP and GFRP as a strengthening measure to mitigate the failure of such SHS members subjected to monotonic and cyclic loading. Monotonic test results are analysed separately for the moment, stiffness and ductility to assess the structural static performance of the bare and strengthened SHS members. From cyclic loading tests, the structural performances of the bare and strengthened SHS members are compared in terms of ultimate moment capacity and moment degradation, stiffness and energy dissipation. A prediction model was also established theoretically to predict the moment capacity of strengthened SHS members under flexural loading. The findings from this study can be used as a guideline for enhancing and restoring the structural integrity of civil infrastructures built using SHS members in the high earthquake-risk zone through CFRP and GFRP strengthening.

2. Experimental investigation

2.1 Materials

Four types of materials were used in the preparation of test specimens: steel, epoxy adhesive, CFRP and GFRP. OneSteel Ltd, Australia distributed the SHS steel (Grade of 350L) members of 100 mm width and height with 3 mm wall thickness in 6000 mm lengths. Standard tensile coupons were tested according to AS 1391 (AS 1391, 2007) to obtain the material properties of the steel and reported in the author's previous study (Tafsirojjaman, Fawzia, Thambiratnam, & Zhao, 2021). Two-part MBrace epoxy adhesives were supplied by BASF

Construction Chemicals Australia Pty Ltd. Material properties of this adhesive was determined and reported in the authors' previous study (Kabir, Fawzia, Chan, Gamage, et al., 2016) using tensile coupons following ASTM: D638-10 (ASTM D638, 2010). CFRP and GFRP were bonded with the steel using the epoxy adhesive to strengthen the SHS. BASF Australia supplied the CFRP while the GFRP was supplied by CG Composite Australia. The material properties in tension for both CFRP and GFRP laminates were determined following ASTM:D3039-08 (ASTM D3039, 2008) and are reported in (I. Alam et al., 2013). The average thicknesses were 0.60 mm and 0.65 mm for the used unidirectional CFRP and GFRP composites respectively. The mechanical properties of steel, epoxy adhesive, CFRP and GFRP are summarised in Table 1.

Table 1: Materials mechanical properties Tafsirojjaman, Fawzia, Thambiratnam, & Zhao, 2021; Kabir, Fawzia, Chan, Gamage, et al., 2016; I. Alam et al., 2013)

Properties	Steel	Adhesive	CFRP	GFRP
Modulus of elasticity (GPa)	190	2.86	75	23
Tensile stress (MPa)	475	46	987	508
Yield stress (MPa)	380	-	-	-

2.2 Experimental Members and Strengthening Scheme

Six SHS members are prepared for evaluation and comparison of monotonic and cyclic behaviour. These specimens are: two bare steel members as the control specimens, two CFRP wrapped, and two GFRP wrapped - one of each type for monotonic and cyclic flexural experiments. All the specimens are cut from lengths of SHS steel, maintaining the same length, width and wall thickness in all members. The adhesive used for the CFRP and GFRP was identical for all strengthened members. Each specimen was named for identification during testing and analysis of results. The first two terms specify either a strengthened beam (SB) or a bare beam (BB). The next term is indicating the use of strengthening material or types where

B is indicating the unstrengthened bare members, C is indicating the strengthening with CFRP and G is indicating the strengthening with GFRP. Finally, the applied loading condition for each member where the monotonic loading is indicated by M and the cyclic loading is indicated by C. The matrix of the experimental specimens is shown in Table 2.

Table 2: Matrix for experimental specimens

Notation	Kinds of member	Strengthening materials	Applied loading
BB-B-M	Bare beam	-	Monotonic
BB-B-C	Bare beam	-	Cyclic
SB-C-M	Strengthened beam	CFRP	Monotonic
SB-C-C	Strengthened beam	CFRP	Cyclic
SB-G-M	Strengthened beam	GFRP	Monotonic
SB-G-C	Strengthened beam	GFRP	Cyclic

Both dry CFRP and GFRP sheets were wrapped by the hand and wet lay-up method. The applied length of the FRPs was 600 mm and placed at the mid-section of SHS to obtain a 300 mm bond length on both sides of the loading point (central) as the previous investigation indicated that a bond length of 300 mm is highly efficient for strengthening steel members (Tafsirojjaman, Fawzia, Thambiratnam, et al., 2020b). The first and second FRP layers were applied identically at the centre of SHS where the FRP fibres orientation was longitudinal (L) along the length of the SHS member. The 600 mm wide third (final) layer was placed directly on top of the second layer with its fibres running laterally or hooped (H) across the member to confine the previous layers of FRPs and have higher resistance against debonding. Each of the FRP layers was overlapped by 75 mm to maintain the continuity of the FRPs. The schematic drawing of the strengthened SHS members is shown in Figure 1.

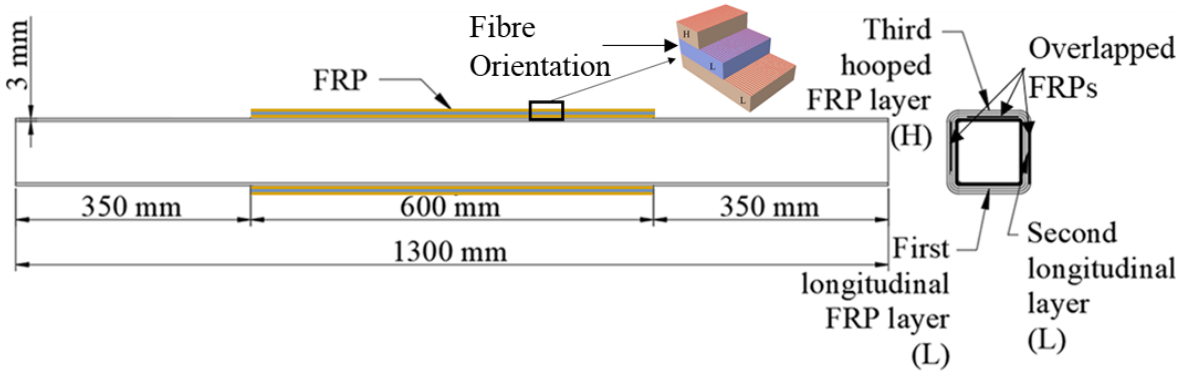

Figure 1: Schematic drawing of strengthened SHS members

2.3 Specimen Preparation and Strengthening Procedure

SHS steel specimens were cut to 1300 mm lengths. The strengthened specimens were then wrapped with either CFRP or GFRP sheets. The first step of the strengthening procedure is the surface preparation of the bonding area. Sandblasting was used to prepare surfaces for the tested SHS specimens. This surface preparation method is found effective in purging impurities from steel surfaces and in preparing high-strength adhesive bonding (Tafsirojjaman, Fawzia, & Thambiratnam, 2019a; Tafsirojjaman, Fawzia, Thambiratnam, & Zhao, 2021; Tafsirojjaman, Fawzia, Thambiratnam, et al., 2019b). Once sandblasted, acetone was used to remove any excess dust from the steel surface. These cleaned members were then coated with the adhesion-promoting two-part epoxy MBrace 3500 primer. This mixture was combined directly before application following the manufacturer's guidelines. To ensure the primer formed a uniform layer the specimens were rotated throughout their curing time. The primer was allowed to cure for 1 hour as per manufacturer guidelines. Then both parts of MBrace 4500 saturant were mixed thoroughly and spread over the primer-coated SHS members. Both FRPs were wrapped by identical methods i.e. in the same location, orientation and method. The FRPs were cut to size and wrapped around the adhesively coated SHS section. Additional coats of MBrace 4500 were applied between each FRP layer and rib-rolled to ensure complete saturation. Each subsequent layer was placed with its starting point opposite to that of the

previous layer to reduce the likelihood of weak points. Once all FRP layers were applied to the specimen, they were wrapped in masking tape to reduce the possibility of premature debonding during the curing process as also implemented in (Tafsirojjaman, Fawzia, & Thambiratnam, 2019a; Tafsirojjaman, Fawzia, Thambiratnam, & Zhao, 2021; Tafsirojjaman, Fawzia, Thambiratnam, et al., 2019b). After 24 hours, the tapes were removed and were allowed the curing of epoxy for a further 14 days. Figure 2 shows different steps of strengthening schemes during specimen preparation as well as all the prepared specimens for testing.

(a)

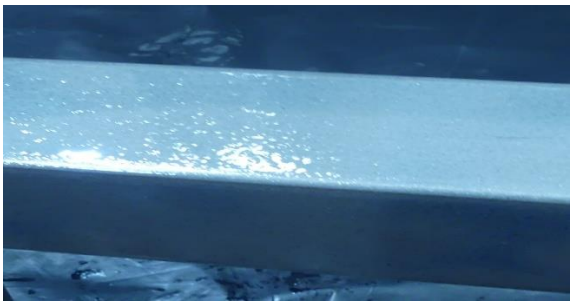

(b)

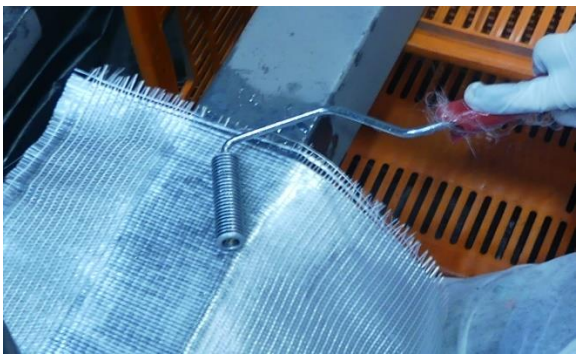

(c)

(d)

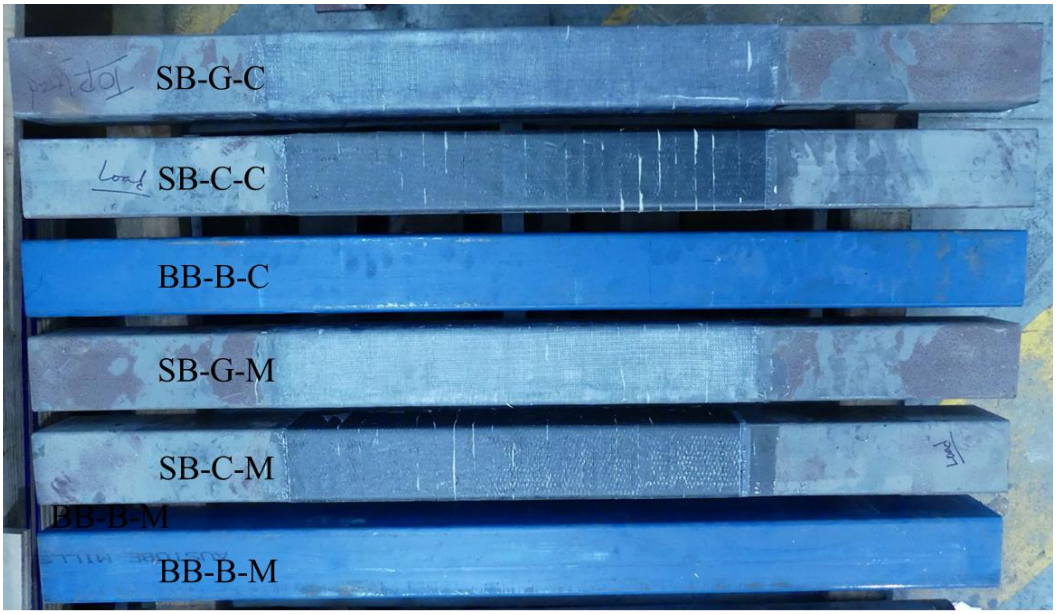

(e)

Figure 2: (a) Sandblasted surface (b) Primer-coated surface (c) Rib-rolling (d) Applying the masking tape (e) Experimental specimens prepared for testing

2.4 Test Setup and Instrumentation

The supports were located at both ends of the SHS member at a test span of 1150 mm. For the monotonic test, both supports were pinned to allow the SHS to sit horizontally in a simply supported condition. A round bar of 20 mm diameter was used as vertical support at each end. Two vertical bars were welded as lateral restraints at each support, one on either side of the member, to keep the test specimen in its lateral position. This approach allowed flexibility in the support, ensuring an accurate test method. The displacement control load was applied to the midspan of the member by a hydraulic actuator of 1000 kN loading capacity and ±300 mm displacement capacity through a round bar of 20 mm diameter, seated below a 16 mm thick plate to distribute the load slightly, as shown in Figure 3. This was done to minimise the probability of crushing the member and FRP due to a concentrated applied load. For the cyclic tests, additional round bars of 20 mm diameter were bolted to the end supports above the member to resist the uplift during the reverse cycle. Another round bar of 20 mm diameter

and a plate of 16 mm thick were bolted to the actuator under the member to transfer the load during reverse cycles in the cyclic tests. To eliminate any deformation due to the loosening of supports and loading assembly, all the used bolts for clipping at both end supports as well as loading assembly were tightened carefully.

The displacement control quasi-static cyclic loading tests were performed by following the ANSI/AISC 341–16 (ANSI/AISC 341-16, 2016) specified large-deformation cyclic loading protocol which can simulate the far-field type earthquake as shown in Figure 5. Far-field earthquakes have some characteristics that differentiate them from near-field earthquakes. Far-field earthquakes have lower acceleration and higher frequencies compared with lower frequencies of near-field earthquakes (Heydari & Mousavi, 2015). It was noticed that high-rise buildings or large structures were highly affected during far-field excitation because of the narrow band nature and long duration of far-field excitation (Ngamkhanong et al., 2018). The cyclic load was applied as a quasi-static rate by following the ANSI/AISC 341–16 (ANSI/AISC 341-16, 2016) and the literature (Al-Bermani et al., 1994; Fadden et al., 2014; Fadden & McCormick, 2011; Z. Li et al., 2011; Tafsirojjaman, Fawzia, Thambiratnam, & Wirth, 2021; Zhou et al., 2017; Zhu et al., 1995). The test setup can be seen clearly in the schematic figure and the actual setup in Figure 3 and Figure 4, respectively. Failure modes of all tested bare and strengthened SHS members can be seen in Figure 6.

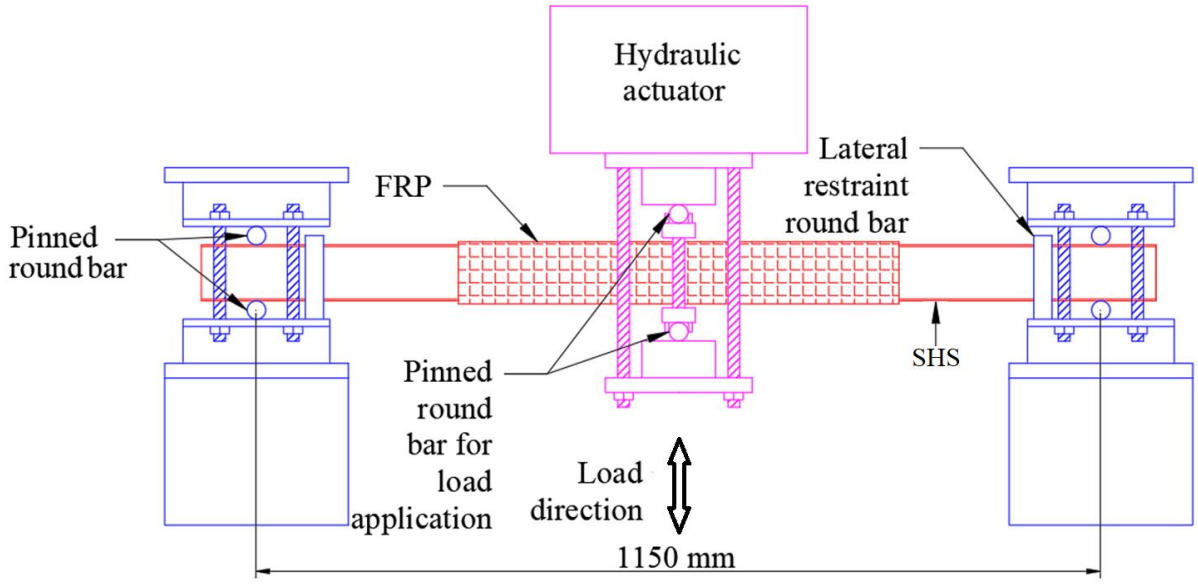

Figure 3: Schematic figure of the test set-up.

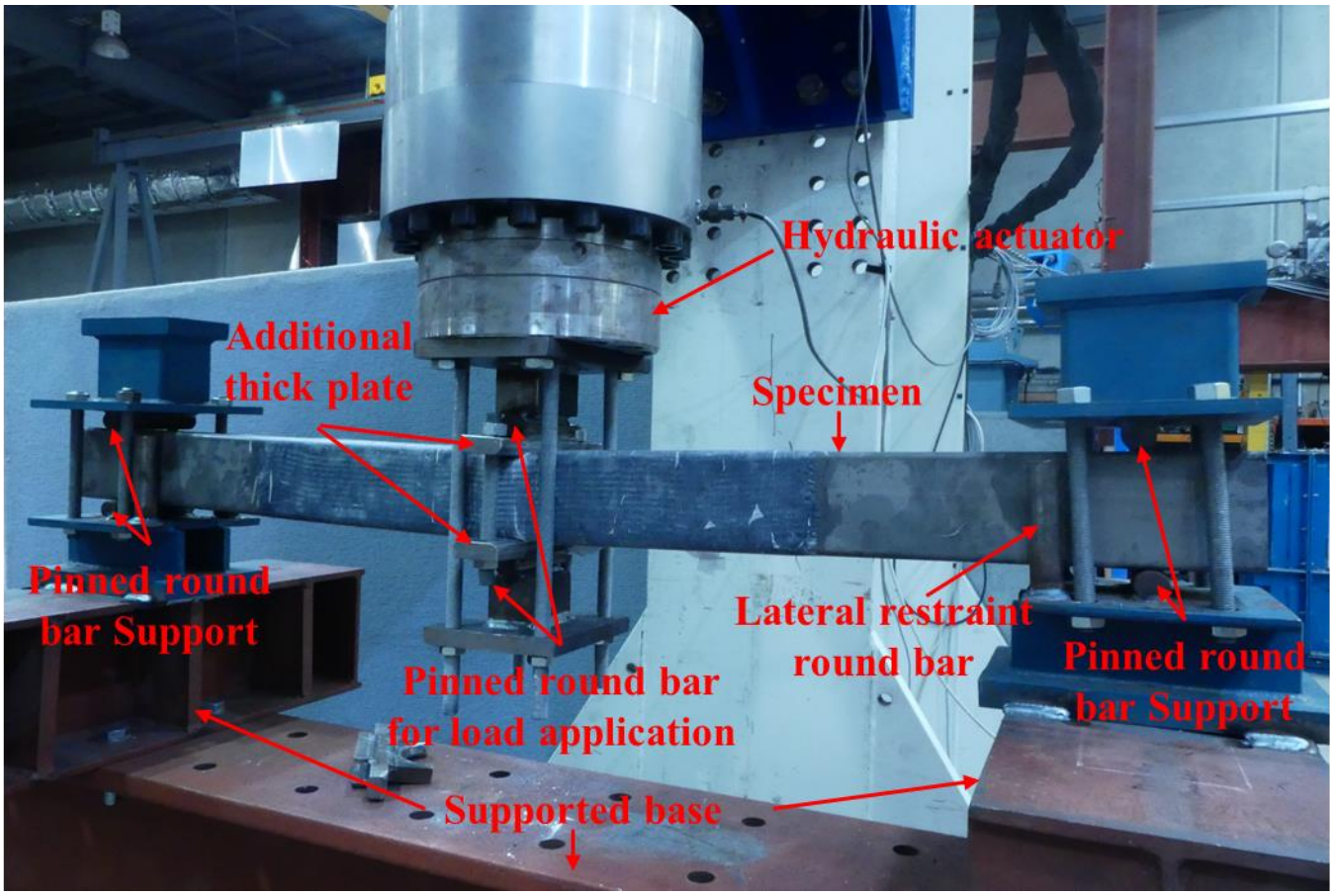

Figure 4: Test set-up.

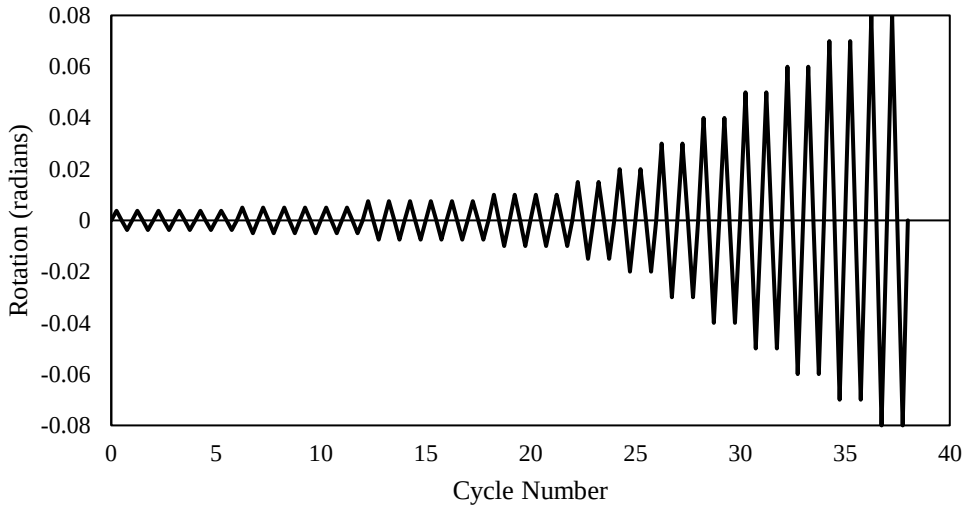

Figure 5: ANSI/AISC 341–16 cyclic loading protocol (ANSI/AISC 341-16, 2016).

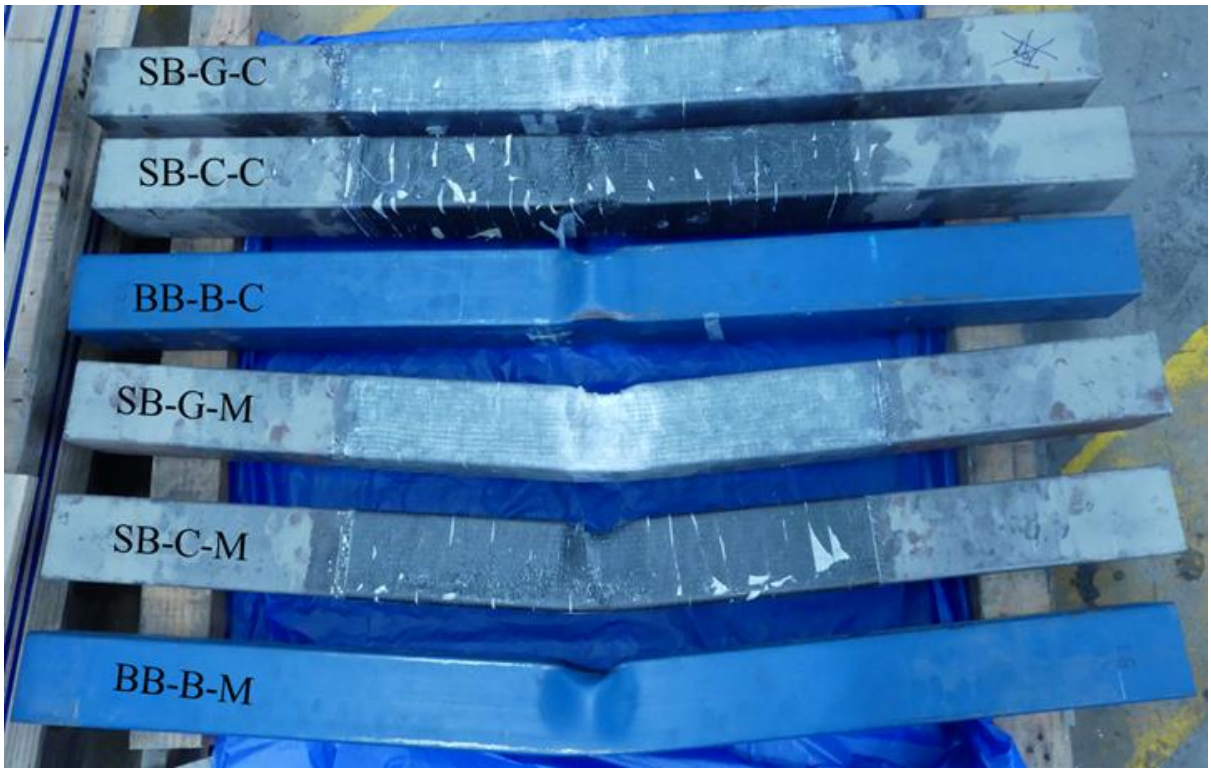

Figure 6: Bare and strengthened SHS specimens after testing.

3. Results and Discussions

The static and cyclic or seismic responses of the SHS members have improved when strengthened by CFRP and GFRP composites. The moment capacity, ductility, secant stiffness and energy dissipation of the SHS member are greatly increased by strengthening with FRP

due to its longitudinal fibres in the direction of the tensile loading and a hooped layer running transversely to confine the longitudinal layers. The detailed responses of the tested specimens are presented in the following sections.

3.1 Structural responses under monotonic loading

Moment capacity-rotational responses were developed for the bare and strengthened SHS members by measuring their moment for a given rotation under monotonic loading. The simply supported member formula for an applied load at the member's centre (*PL/4*), where the load (*P*) and the span length (*L*) which is the clear distance between supports (1.15 m), are used to obtain the moment capacity (Tafsirojjaman, Fawzia, Thambiratnam, & Wirth, 2021). Moreover, the rotational capacity means the capability of the member able to carry the level of rotation and is predicted by dividing the applied midspan displacement by half of the span length (*L*) (Tafsirojjaman, Fawzia, Thambiratnam, & Wirth, 2021).

The moment capacity-rotation curves under monotonic loading for the tested bare and strengthened SHS specimens were shown in Figure 7 where the strengthened SHSs show greater moment capacity in contrast to the bare steel SHS specimen. The bare, CFRP and GFRP strengthened SHS steel members' ultimate moment capacities are 15.2 kNm, 18.5 kNm and 16.4 kNm respectively. Hence, both FRP strengthening techniques increases the ultimate moment capacity of SHS steel member. These increases are 21.2% under CFRP strengthening and 7.8% under GFRP strengthening. The additional strength provided by FRP and the confinement effect of composites played a major role in enhancing the moment capacity of SHS members. Moreover, the CFRP with the almost same amount of fibres can result in a higher capacity section due to having higher strength material properties compared to GFRP. Additionally, at the ultimate moment capacity points, the strengthened members had greater rotational capacities. At their ultimate moment capacities, the CFRP and GFRP-strengthened

members were shown the rotational capacity of 0.02 radians and 0.016 radians respectively while the bare member was shown the rotational capacity of 0.014 radians.

Figure 6 shows the comparisons of all three types of members after testing under monotonic loading. It is evident that both strengthened members demonstrate less tendency for buckling and result in higher rotational capacities compared to the bare member. These results confirmed that both FRP strengthening techniques can improve the structural behaviours of SHS members subjected to monotonic loading effectively. Moreover, typical ductile modes of failure were exhibited by all of the bare and FRP-strengthened members. This can be explained by similar failure behaviour observed wherein the prominent failure mode was the local buckling at the middle of the member in the compression zone (Tafsirojjaman, Fawzia, Thambiratnam, & Wirth, 2021). Moreover, the FRP composites were debonded in the compression zone which might be due to high compressive stress and buckling in the compression zone. Furthermore, the FRP composites were crushed after the ultimate loading at the middle of both FRP-strengthened members in the compression zone. This might be due to the stress concentration at the edge of the rigid steel plate where the rigid steel plate was used to apply the displacement, as well as the FRPs at this area, which was already weakened after debonding. Similar failure modes were noticed during the investigation of the structural behaviour of the CFRP and GFRP-strengthened CHS beams subjected to monotonic and cyclic loadings (Tafsirojjaman, Fawzia, Thambiratnam, & Wirth, 2021). The FRP composites were applied with sufficient bond length as both CFRP and GFRP composites remained intact at end of wrapping and in the tension zone.

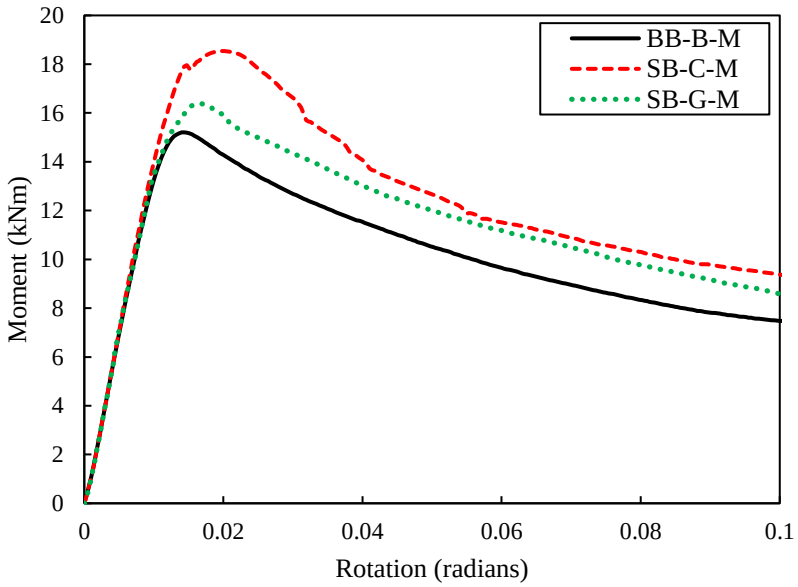

Figure 7: Moment-rotational responses under monotonic loading.

The secant stiffness, calculated as the ratio of the applied load to the corresponding displacement is plot versus displacement (Figure 8), for all three types of SHS steel members under monotonic loading. The secant stiffness of the beams is initially ascending due to the initial deformation adjustment of the support and loading assembly. The same type of behaviour has been reported in the literature (Fadden & McCormick, 2011; Tafsirojjaman, Fawzia, Thambiratnam, & Zhao, 2021). All beams experienced a decline in secant stiffness under increased rotation. Secant stiffness of the CFRP-strengthened member was 686.8 kN/m while that of the GFRP-strengthened member was 650.7 kN/m at their ultimate rotational levels. In contrast to the bare SHS member's secant stiffness of 551.6 kN/m at the ultimate rotational level, these are 24.5% and 17.9% respectively enhancements as a result of the strengthening with CFRP and GFRP. In addition, the strengthened SHS beams with CFRP and GFRP had the highest secant stiffness of 8677.6 kN/m and 8542.0 kN/m respectively. These represent an increase of 3.0% due to strengthening with CFRP and 1.4% due to strengthening with GFRP over the maximum secant stiffness of 8418.6 kN/m of the bare SHS member. The higher stiffness material characteristics of the CFRP composite than the GFRP composite

resulted in the CFRP-strengthened SHS member having a greater secant stiffness compared to the GFRP-strengthened SHS member.

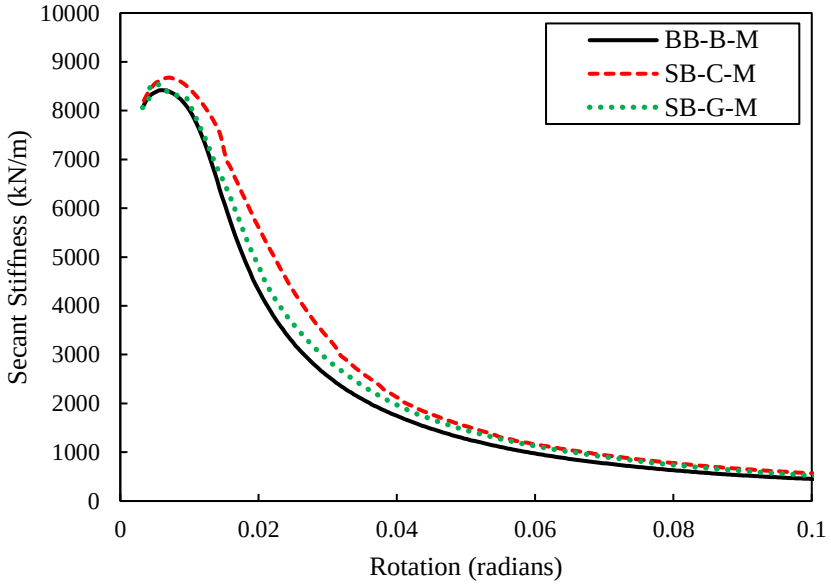

Figure 8: Secant stiffness-rotational responses under monotonic loading.

The seismic performance of the steel structure is significantly affected by the ductility of the members in the steel frame. The ductility index, therefore, needs to be studied in the overall performance of the strengthened members. The ductility index of the members can be expressed by the ratio of ultimate lateral displacement (δ_u) and the yield lateral displacement (δ_y) (Tafsirojjaman, Fawzia, Thambiratnam, et al., 2019a) where δ_u is the lateral displacement corresponding to the 90% of the ultimate load (Tafsirojjaman, Fawzia, Thambiratnam, et al., 2019a) and δ_y is obtained according to Li et al. (Z. X. Li, 2004). Figure 9 displays the ductility index of the bare and FRP-strengthened beams. The improvements in the ductility index can be seen due to both FRP strengthening methods. The bare, CFRP and GFRP-strengthened specimens were shown ductility indexes of 1.94, 2.19 and 2.17 respectively. Hence, for CFRP and GFRP strengthening there was 12.4% and 11.5% respectively enhancement in the ductility index which isn't a significant enhancement but satisfactory. Those enhancements in the ductility index are the direct result of the enhanced post-yield properties of the FRP-

strengthened members. Moreover, the strengthened FRPs in the hoop directions offer better restraint of the steel member so that the ductility of the restrained steel is enhanced which has been concluded by Haedir et al. [55] as well.

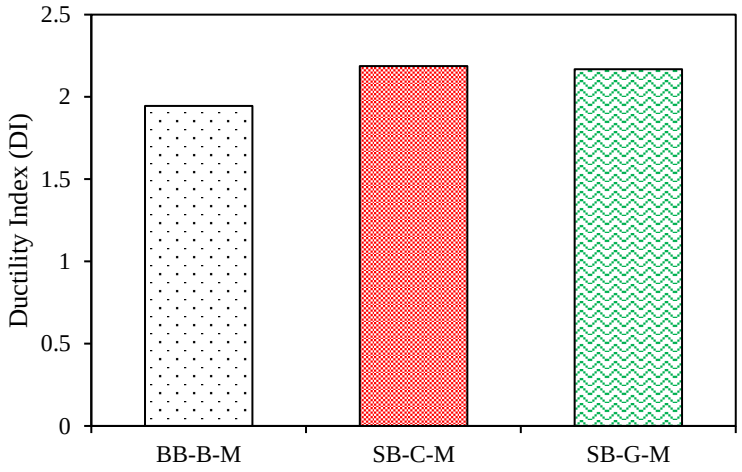

Figure 9: Ductility index

3.2 Structural responses under cyclic loading

The structural cyclic or seismic responses of the CFRP and GFRP-strengthened SHS were analysed and the moment hysteresis, moment degradation, secant stiffness and energy dissipation capacity, and were compared with those of the bare steel SHS. The experimental results showed that both FRP strengthening methods had significant effects on the structural performances of SHS members. The effects of both FRP strengthening techniques on various structural performances are discussed in the following sections.

3.2.1 Hysteresis behaviour

The cyclic hysteresis behaviour of the bare and strengthened SHS members was analysed through the moment-rotation hysteresis behaviour and the results are shown in Figure 10 (a), (b) and (c) respectively. A flat portion on the graphs at zero loads after the yield is seen in each cycle where the hydraulic actuator moved without applying a load. This flat section is

due to the formation of plastic deformation at mid-span with zero moment capacity. An inelastic response is observed in the experimental results for all three types of members. After the yield, the second cycle for each level of rotation had a reduced moment capacity, which was further reduced with each subsequent cycle as the yielding of the steel member was seen. The moment capacity was reduced further when the rotations were increased. The moment capacities of the cyclically loaded strengthened members were higher than that of the bare steel SHS. The ultimate moment capacities in the positive direction for the bare, CFRP and GFRP-strengthened members were 14.5 kNm, 17.8 kNm and 16.7 kNm, respectively. This gives an increase in ultimate moment capacity over the bare member of 22.5% for the CFRP-strengthened SHS and 15.0% for the GFRP-strengthened SHS. In the negative rotation, the strengthened members showed greater ultimate moment capacities than their bare counterparts. In the negative direction, the ultimate moment capacity of the bare, CFRP and GFRP-strengthened SHS was 15.1 kNm, 17.6 kNm and 16.0 kNm, respectively. These values correspond to increases of 16.9% and 6.1% due to CFRP and GFRP strengthening respectively compared to the bare steel SHS. The strengthened SHS members had a larger ultimate moment capacity in the positive rotation than in the negative rotation. At the ultimate moment capacity, the rotational levels were 0.01 radians for the bare, 0.015 radians for CFRP and 0.015 radians for the GFRP-strengthened members in both rotational ways. Hence, an increased level of rotation in both FRP strengthened SHSs due to their increased ductility and less local bucking potential than bare steel member. In addition, a similar failure mode was shown by all of the bare and strengthened beams wherein the failure mode was the local buckling at the middle of the member as shown in Figure 6. Moreover, the FRP composites in both types of FRP-strengthened members were debonded and crushed at the middle of the member in both of bottom and top surfaces. This failure mode resulted due to the applied push and pull loading effect throughout the cyclic loading testings which can be seen in Figure 6. However, FRP

composites were intake and no debonding was noticed at the end of the FRP composites in both FRP-strengthened members.

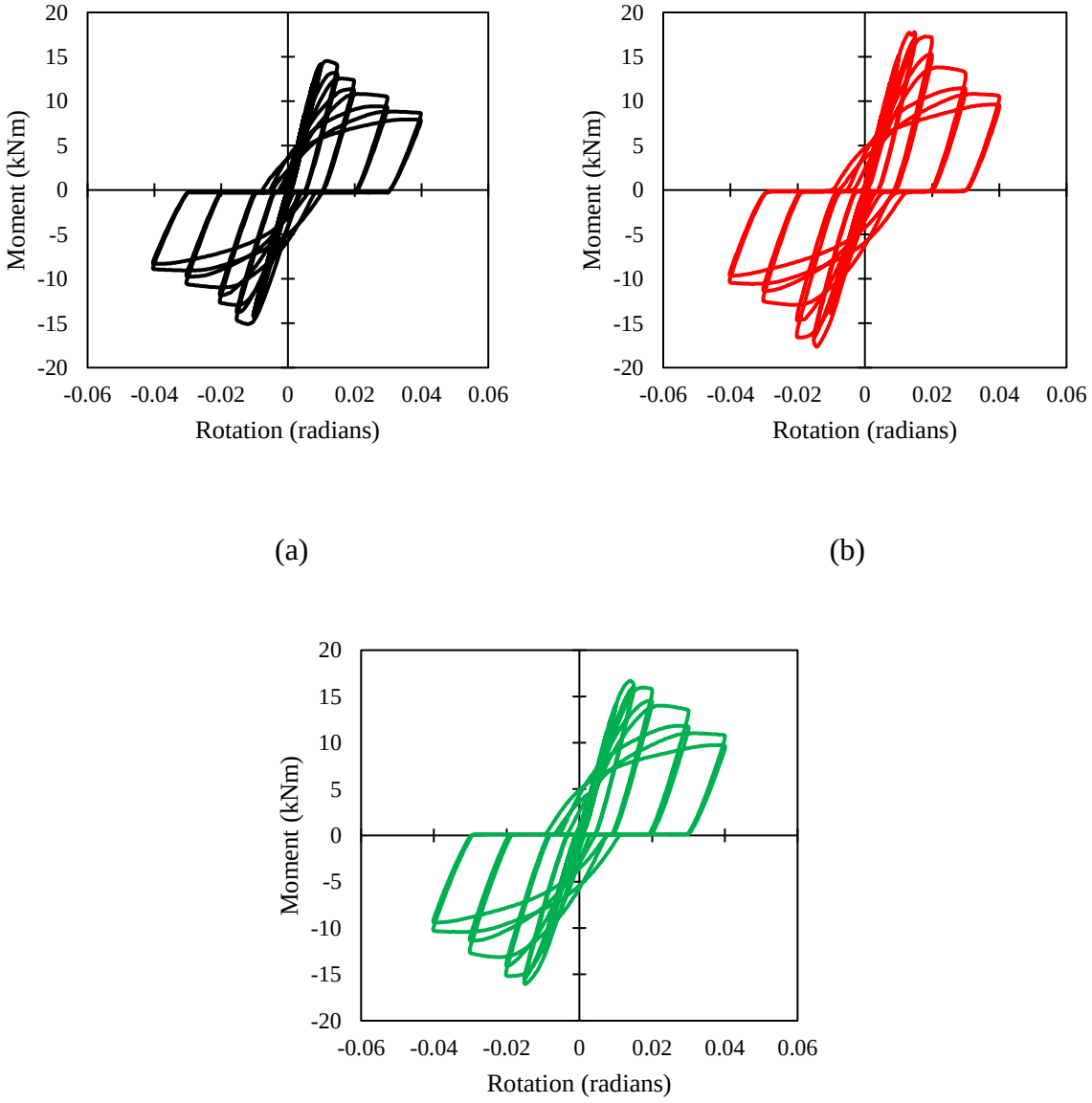

Figure 10: Moment-rotational hysteresis responses of the (a) bare (b) CFRP and (c) GFRP-strengthened SHS members

3.2.2 Moment Degradation Response

The moment degradation responses for the bare and strengthened SHSs were analysed through the backbone curves of moment-rotation hysteresis responses. The plots shown in

Figure 11 represent the moment at the highest rotation for the initial cyclic sequence at each rotational level. From the figure, it can be seen that there is a closely symmetric response in the positive and negative rotations for each of the tested members. After achieving their ultimate moment capacities, the three tested members displayed a reduction in moment capacity for the consequent rotational level due to the degradation of the material's stiffness. The moment degradation for each member is caused by the local buckling of the steel SHS. SHS members strengthened with CFRP and GFRP showed greater moment capacities than SHS alone even after yielding at maximum rotation levels for higher rotation levels. For the positive direction rotations, the bare SHS member had an ultimate moment capacity of 14.2 kNm at the rotation of 0.01 radians and decreased to 8.7 kNm at the utmost rotation of 0.04 radians. For the CFRP-strengthened SHS member, the ultimate moment capacity was 17.6 kNm at the rotational level of 0.015 radians and reduced to 10.5 kNm at its utmost rotation of 0.04 radians. For the GFRP-strengthened SHS member, the ultimate moment capacity was 16.3 kNm at 0.015 radians and reduced to 10.8 kNm at its utmost rotation of 0.04 radians. Hence, CFRP and GFRP-strengthened SHS members exhibited 21.0% and 24.3% respectively higher moment capacities in contrast to the bare SHS at the utmost rotation of 0.04 radians. Although the CFRP-strengthened SHS member had shown greater ultimate moment capacity than the GFRP-strengthened SHS member, the GFRP-strengthened SHS member had a greater moment capacity at the utmost rotation of 0.04 radians. Hence, GFRP-strengthened SHS member exhibited lower moment degradation than CFRP-strengthened SHS member. This can be due to the lower stiffness of GFRP and its better capacity to absorb cyclic forces than that of CFRP. All three types of members show almost identical moment degradation responses in the negative rotation as was also seen in the positive direction.

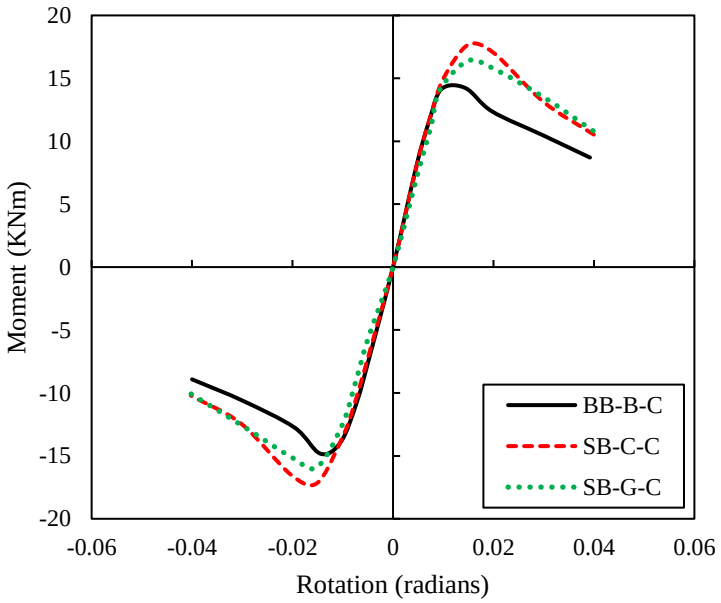

Figure 11: Backbone curves of the cyclic hysteresis curves

3.2.3 Secant Stiffness

The load capacity at the maximum displacement of the particular rotational level was divided by that displacement to calculate the secant stiffness for that particular level of rotation. The secant stiffness-rotational responses for bare and strengthened members are displayed for comparison in Figure 12. It is evident that the secant stiffness reduced in all three types of members with the increase in rotational level due to the yielding of the steel. Secant stiffness behaviours of bare and strengthened steel members are nearly symmetrical in the positive and negative rotational directions. While all the members had gradual reductions in stiffness, both FRP-strengthened SHS members had lower stiffness degradation compared to their bare steel counterparts. At the maximum rotation of 0.04 radians, the degradation of stiffness was 84.9% for the bare steel SHS, 82.3% for the CFRP-strengthened member and 82.0% for the GFRP-strengthened member from their maximum stiffness. Therefore, CFRP and GFRP strengthening enhanced the stiffness of SHS members due to the additional confinement and strength given by the CFRP and GFRP. Additionally, the secant stiffness of the CFRP and

GFRP-strengthened SHS members is 18.6% and 22.4% respectively higher than the bare counterpart at the maximum positive rotation of 0.04 radians. Similarly, the CFRP and GFRP-strengthened SHS members show higher secant stiffness of 13.6% and 12.5% respectively over the bare member in the maximum negative rotation of 0.04 radians.

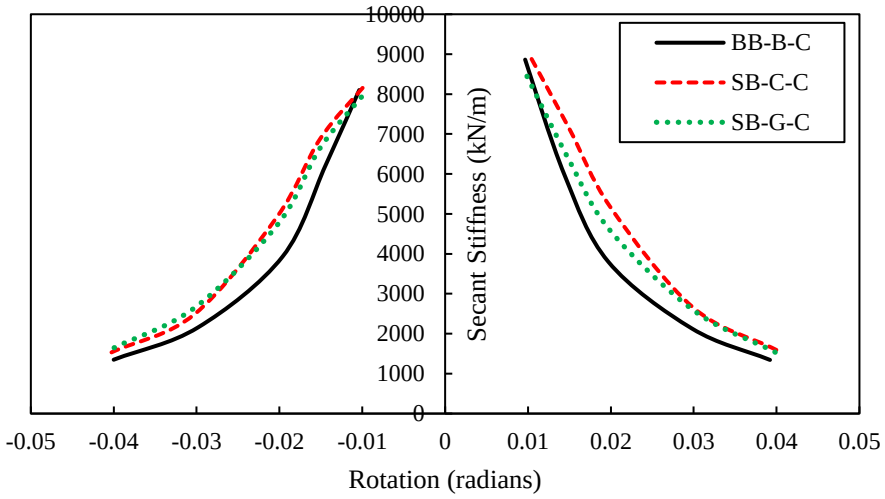

Figure 12: Secant stiffness-rotational responses under cyclic loading

3.2.4 Energy Dissipation Capacity

An investigation into the impact of both FRP materials on the energy dissipation capacity of cyclically loaded SHS was carried out. The majority of seismic energy applied to a structure is dissipated through the inelastic deformation of structural elements. The structural elements that inelastically deform in a steel frame building are usually the beams, the base of a column, and internal panels. Therefore, when designing for earthquake loadings, it is critical to consider the capacity for energy dissipation of both strengthened and unstrengthened steel members. The area encircled by all cycles for all rotation levels is plotted versus the level of rotation to determine the energy dissipation for each member. Energy dissipation capacities for bare, CFRP and GFRP-strengthened SHS members are presented in Figure 13. The dissipated energy by all members was minimal within their elastic region of up to around 0.0075 radians.

Further, the strengthened members had a lower energy dissipation than the bare beam for up to 0.02 radians of rotation due to the stiffness and confinement contribution by FRP strengthening. However, after the beams yielded, while the energy dissipation rapidly increased, both strengthened members increased at a higher rate in contrast to the bare member. At maximum rotation of 0.04 radians, the dissipated energy was 2.10 kNm for the bare member, 2.53 kNm for the CFRP-strengthened member and 2.50 kNm for the GFRP-strengthened member. These were increments of 20.6% for the CFRP-strengthened member and 19.1% for the GFRP-strengthened member compared to the bare steel section. Therefore, both FRP strengthening enhances the almost same level of energy dissipation capacity, although CFRP strengthening is more efficient to enhance the strength of the SHS member compared to GFRP strengthening. This behaviour has been noticed as both FRP-strengthened members have almost the same ductility capacity and the lower stiffness material properties of GFRP also have additional effects to enhance the energy dissipation capacity as well.

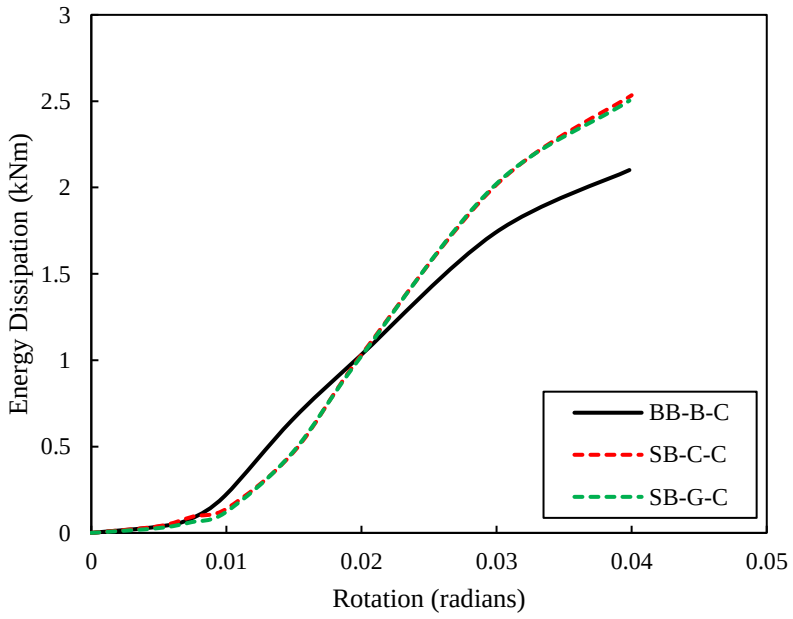

Figure 13: Energy dissipation-rotational responses under cyclic loading

4. Theoretical prediction model

The ultimate moment capacity of the bare SHS members can be predicted by following AS4100 (*AS 4100: Steel Structures*, 1998). On the other hand, a theoretical model to predict the ultimate moment capacity of FRP-strengthened steel SHS members was developed based on AS4100 (*AS 4100: Steel Structures*, 1998) and Haedir et al. (Haedir et al., 2009). The equivalent steel section approach proposed by Haedir et al. (Haedir et al., 2009) for the FRP-strengthened circular hollow section is implemented to transform the FRP strengthened SHS into equivalent steel SHS section. The thickness of the supplemented area of FRP to steel ($t_{es}^{(cs)}$) was calculated by assuming that there will be no debonding and failure of the FRP before reaching the ultimate moment capacity in addition to the influence of the modular ratio concept and the percentage of the fibre strength efficiency relative to steel according to Haedir et al. (Haedir et al., 2009). For the FRP-strengthened SHS section, the transformed section of the FRP-strengthened SHS section is shown in Figure 14.

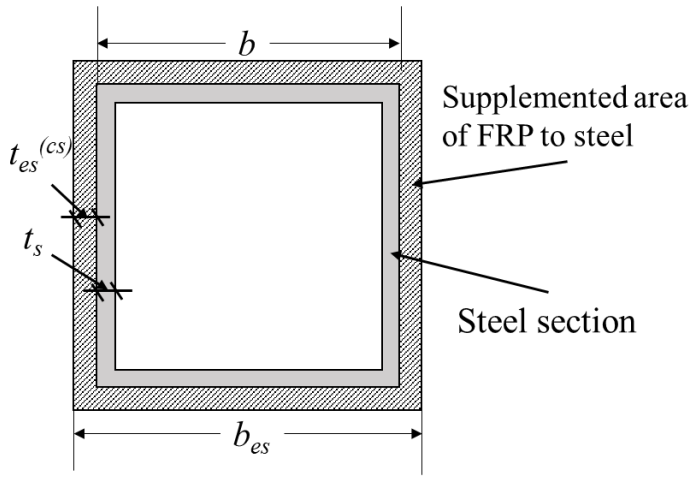

Figure 14: Transformed section of FRP-strengthened SHS section

From this transformed section of FRP-strengthened SHS section, the equivalent elastic section modulus (Z_{es}) and equivalent plastic section modulus (S_{es}) can be obtained by Equation (1) (Dym & Shames, 1973) and Equation (2) (Dym & Shames, 1973) respectively and given below:

$$Z_{es} = \frac{b_{es}{}^4 - (b_{es} - 2t_{es})^4}{6b_{es}} \quad (1)$$

$$S_{es} = \frac{b_{es}{}^3 - (b_{es} - 2t_{es})^3}{4} \quad (2)$$

In the above equations, the dimensions of the equivalent section are $b_{es} = b + 2t_{es}^{(cs)}$ and $t_{es} = t_s + t_{es}^{(cs)}$.

Then, the ultimate moment capacity of the FRP-strengthened SHS section ($M_b^{(SS)}$) under bending can be predicted by using Equation (3) (Dym & Shames, 1973) theoretically and given below:

$$M_b^{(SS)} = Z_{ese}\, \sigma_y^{(s)} \quad (3)$$

where Z_{ese} refers to the effective section modulus of the equivalent steel section and $\sigma_y^{(s)}$ refers to the yield strength of the steel. For the compact SHS section, the effective section modulus is equal to the equivalent plastic section modulus.

The local buckling at the middle of the member in the compression zone was the prominent failure mode and the FRP composites remained intact at end of wrapping for all the FRP-strengthened specimens. Hence, although only a portion of the beams is strengthened with FRP, it does not influence the ultimate moment capacity as the FRP act as an effective composite material with the steel SHS and the section modulus of the middle of the section has played the key factor on the ultimate moment capacity. The effective section modulus of the midsection has been considered to predict the ultimate moment capacity. Table 3 compares the experimental and predicted moment capacity of the bare, CFRP and GFRP-strengthened members. It is evident that the two sets of results match well for all the bare, CFRP and GFRP-strengthened members. Moreover, the actual ultimate stresses on the CFRP and GFRP composites were 179.9 MPa and 53.0 MPa respectively which were much lower than the actual

ultimate stress on the steel SHS (416.2 MPa) under monotonic loading. Almost similar stresses were exhibited by steel SHS, CFRP and GFRP under cyclic loading. Hence, the ultimate capacity of the FRP-strengthened members has been dominated by the buckling of the steel SHS and failure of the FRP will not occur before reaching at the ultimate moment capacity. The effect of cyclic loading has not been considered in the current prediction model due to the limitation of data which is out of the scope of the current study and can be considered for future study.

Table 3: Comparison of experimentally obtained and theoretically predicted results

Specimen identifier	Ultimate Moment capacity (kNm)		$\frac{M_{EXP}}{M_{Theo}}$
	Theoretical (M_{Theo})	Experimental (M_{Exp})	
BB-B-M	14.19	15.21	0.93
SB-C-M	18.50	18.54	1.00
SB-G-M	16.89	16.40	1.03
BB-B-C	14.19	15.10	0.94
SB-C-C	18.50	17.80	1.04
SB-G-C	16.89	16.73	1.01
		Mean	0.99
		COV	0.04

5. Conclusions

The structural responses of the bare and FRP-strengthened SHS members under monotonic and cyclic flexural loading were investigated experimentally. A prediction model was also established theoretically to predict the moment capacity of strengthened SHS members under flexural loading. The following conclusions can be drawn based on the present investigation:

i. CFRP and GFRP strengthening increased the ultimate moment capacity of the SHS member due to the additional strength provided by FRP and the confinement effect of composites. The increase is 21.9% for CFRP and 7.8% for GFRP indicating that the CFRP with the almost same amount of fibres can result in a higher capacity section due to having higher strength material properties compared to GFRP as well as high confinement.

ii. CFRP-strengthened member had a bit higher second stiffness compared to the GFRP as CFRP has higher strength and stiffness than GFRP. However, the ductility of the GFRP-strengthened member is very close to the CFRP-strengthened member as lower stiffness of GFRP provides more advantages for having a better enhancement of ductility behaviour than that of CFRP.

iii. The enhancements of the ultimate moment capacities of SHS members under cyclic loading due to CFRP and GFRP strengthening techniques are higher than under monotonic loading. This can be due to the additional confinement and ductility by FRP which reduces the cyclic vulnerability of members greatly by increasing the energy absorption capacity.

iv. Both strengthened SHS members demonstrated higher ductility and less tendency for buckling which result in higher rotational capacities at their ultimate moment capacity compared to the bare SHS member.

v. Under cyclic loading, the GFRP-strengthened SHS member exhibited lower moment degradation than the CFRP-strengthened SHS member as GFRP is less stiff than the CFRP.

vi. Although CFRP strengthening is more efficient to enhance the strength of the SHS member compared to GFRP strengthening, both CFRP and GFRP strengthening enhance the almost same level of energy dissipation capacity as the lower stiffness

material properties of GFRP also have additional effect to enhance the energy dissipation capacity.

vii. GFRP is found to be more effective than CFRP to strengthen the SHS under cyclic loading. Although the CFRP composite is more than three times stiffer than the GFRP composite, the cyclic performance of the GFRP-strengthened member was close to the CFRP-strengthened member as the performances were dominated by the buckling of the steel SHS and additionally, GFRP has the lower stiffness and better capacity to absorbed cyclic forces than that of CFRP.

viii. The theoretical prediction model was developed by assuming that the FRP will not be debonded and fail before reaching at the ultimate moment capacity in addition to the influence of the modular ratio concept and the modest contribution of the fibre strength. There was good agreement between the theoretically predicted and experimental values of the ultimate moment capacities for all the bare, CFRP and GFRP-strengthened members.

Furthermore, the effect of the number of layers and bond length on the performance of FRP-strengthened SHS as well as FRP-strengthened concrete-filled circular hollow section and the square hollow section can be investigated in future studies through detailed experimental study and numerical investigation such as finite element modelling.

Declaration of competing interest:

The authors declare that they have no known competing financial interests or personal relationships that could have appeared to influence the work reported in this paper.

Data availability statement:

The raw/processed data required to reproduce these findings cannot be shared at this time as the data also forms part of an ongoing study.

Acknowledgement

The authors would like to acknowledge the provided financial funding by the School of Civil and Environmental Engineering of the Queensland University of Technology (QUT), Australia to conduct the current experimental study. The authors would like to thank the technical staff of QUT Banyo Pilot Plant Precinct and Mr. Mingh Kim for their assistance during the experimental works.

Reference

Accord, N. B., & Earls, C. J. (2006). Use of Fiber-Reinforced Polymer Composite Elements to Enhance Structural Steel Member Ductility. *Journal of Composites for Construction*, *10*(August), 337–344. https://doi.org/10.1061/(ASCE)1090-0268(2006)10:4(337)

Alam, I., Fawzia, S., Zhao, X., Asce, F., & Remennikov, A. M. (2013). *Experimental Study on FRP-Strengthened Steel Tubular Members under Lateral Impact*. *21*(5). https://doi.org/10.1061/(ASCE)CC.1943-5614.0000801.

Alam, M. I., Fawzia, S., Tafsirojjaman, T., & Zhao, X. L. (2017). FE modeling of FRP strengthened CHS members subjected to lateral impact. *Tubular Structures XVI: Proceedings of the 16th International Symposium for Tubular Structures (ISTS 2017, 4-6 December 2017, Melbourne, Australia)*, 409–414.

Al-Bermani, F. G. A., Li, B., Zhu, K., & Kitipornchai, S. (1994). Cyclic and seismic response of flexibly jointed frames. *Engineering Structures*, *16*(4), 249–255. https://doi.org/10.1016/0141-0296(94)90064-7

ANSI/AISC 341-16. (2016). *Seismic Provisions for Structural Steel Buildings*. American Institute of Steel Construction.

AS 1391. (2007). *Metallic materials-Tensile testing at ambient temperature*. Standards Australia.

AS 4100: Steel structures. (1998). Standards Australia.

ASTM D638. (2010). *Standard Test Method for Tensile Properties of Plastics.* ASTM Standards.

ASTM D3039. (2008). *Standard Test Method for Tensile Properties of Polymer Matrix Composite Materials*. ASTM Standards.

Azevedo, J., & Calado, L. (1994). Hysteretic behaviour of steel members: Analytical models and experimental tests. *Journal of Constructional Steel Research*, *29*(1–3), 71–94. https://doi.org/10.1016/0143-974X(94)90057-4

Batuwitage, C., Fawzia, S., Thambiratnam, D. P., Tafsirojjaman, T., Al-Mahaidi, R., & Elchalakani, M. (2017). CFRP-wrapped hollow steel tubes under axial impact loading. *Tubular Structures XVI: Proceedings of the 16th International Symposium for Tubular Structures (ISTS 2017, 4-6 December 2017, Melbourne, Australia)*, 401–408.

Charalampakis, A. E., Tsiatas, G. C., & Tsopelas, P. (2019). A mass-reduction design concept for seismic hazard mitigation. *Earthquake Engineering & Structural Dynamics*.

Domaneschi, M. (2012). Experimental and numerical study of standard impact tests on polypropylene pipes with brittle behaviour. Proceedings of the Institution of Mechanical Engineers, Part B: Journal of Engineering Manufacture, 226(12), 2035–2046.

Dym, C. L., & Shames, I. H. (1973). *Solid mechanics*. Springer.

El Damatty, A. A., Abushagur, M., & Youssef, M. A. (2003). Experimental and analytical investigation of steel beams rehabilitated using GFRP sheets. *Steel and Composite Structures*, *3*(6), 421–438. https://doi.org/10.12989/scs.2003.3.6.421

Fadden, M., & McCormick, J. (2011). Cyclic Quasi-Static Testing of Hollow Structural Section Beam Members. *Journal of Structural Engineering*, *138*(5), 561–570. https://doi.org/10.1061/(asce)st.1943-541x.0000506

Fadden, M., Wei, D., & McCormick, J. (2014). Cyclic Testing of Welded HSS-to-HSS Moment Connections for Seismic Applications. *Journal of Structural Engineering*, *141*(2), 04014109. https://doi.org/10.1061/(asce)st.1943-541x.0001049

Feng, M. Q., & Mita, A. (1995). Vibration control of tall buildings using mega subconfiguration. *Journal of Engineering Mechanics*, *121*(10), 1082–1088.

Gao, X. Y., Balendra, T., & Koh, C. G. (2013). Buckling strength of slender circular tubular steel braces strengthened by CFRP. *Engineering Structures*, *46*, 547–556. https://doi.org/10.1016/j.engstruct.2012.08.010

Guha-Sapir, D., Below, R., & Hoyois, P. (2015). EM-DAT: International disaster database. *Catholic University of Louvain: Brussels, Belgium*.

Haedir, J., Bambach, M. R., Zhao, X. L., & Grzebieta, R. H. (2009). Strength of circular hollow sections (CHS) tubular beams externally reinforced by carbon FRP sheets in pure bending. *Thin-Walled Structures*, *47*(10), 1136–1147. https://doi.org/10.1016/j.tws.2008.10.017

Harries, K. A., Peck, A. J., & Abraham, E. J. (2009). Enhancing stability of structural steel sections using FRP. *Thin-Walled Structures*, *47*(10), 1092–1101. https://doi.org/10.1016/j.tws.2008.10.007

Heydari, M., & Mousavi, M. (2015). The comparison of seismic effects of near-field and far-field earthquakes on relative displacement of seven-storey concrete building with shear wall. *Current World Environment*, *10*(Special Issue), 40.

Kaan, B. N., Alemdar, F., Bennett, C. R., Matamoros, A., Barrett-Gonzalez, R., & Rolfe, S. (2012). Fatigue enhancement of welded details in steel bridges using CFRP overlay elements. *Journal of Composites for Construction*, *16*(2), 138–149. https://doi.org/10.1061/(ASCE)CC.1943-5614.0000249

Kabir, M. H., Fawzia, S., & Chan, T. H. T. (2016). Durability of CFRP strengthened circular hollow steel members under cold weather: Experimental and numerical investigation. *Construction and Building Materials*, *123*, 372–383. https://doi.org/10.1016/j.conbuildmat.2016.06.116

Kabir, M. H., Fawzia, S., Chan, T. H. T., & Gamage, J. C. P. H. (2016). Comparative durability study of CFRP strengthened tubular steel members under cold weather. *Materials and Structures*, *49*(5), 1761–1774. https://doi.org/10.1617/s11527-015-0610-x

Kabir, M. H., Fawzia, S., Chan, T. H. T., Gamage, J. C. P. H., & Bai, J. B. (2016). Experimental and numerical investigation of the behaviour of CFRP strengthened CHS beams subjected to bending. *Engineering Structures*, *113*, 160–173. https://doi.org/10.1016/j.engstruct.2016.01.047

Kadhim, M. M. A., Wu, Z., & Cunningham, L. S. (2018). Loading rate effects on CFRP strengthened steel square hollow sections under lateral impact. *Engineering Structures*, *171*(April), 874–882. https://doi.org/10.1016/j.engstruct.2018.04.066

Keykha, A. H. (2019). Structural performance evaluation of deficient steel members strengthened using CFRP under combined tensile, torsional and lateral loading. *Journal of Building Engineering*, *24*, 100746.

Li, Z., Albermani, F., Chan, R. W. K., & Kitipornchai, S. (2011). Pinching hysteretic response of yielding shear panel device. *Engineering Structures*, *33*(3), 993–1000. https://doi.org/10.1016/j.engstruct.2010.12.021

Li, Z. X. (2004). Theory and technique of engineering structure experiments. *Tianjin University Press Tianjin*.

Liu, Y., Tafsirojjaman, T., Dogar, A. U. R., & Hückler, A. (2020). Shrinkage behavior enhancement of infra-lightweight concrete through FRP grid reinforcement and development of their shrinkage prediction models. *Construction and Building Materials*, *258*(119649). https://doi.org/10.1016/j.conbuildmat.2020.119649

Liu, Y., Tafsirojjaman, T., Dogar, A. U. R., & Hückler, A. (2021). Bond behaviour improvement between infra-lightweight and high strength concretes using FRP grid reinforcements and development of bond strength prediction models. *Construction and Building Materials*, *270*, 121426. https://doi.org/10.1016/j.conbuildmat.2020.121426

Liu, Y., Xie, J. Z., Tafsirojjaman, T., Yue, Q. R., Tan, C., & Che, G. J. (2022). CFRP lamella stay-cable and its force measurement based on microwave radar. *Case Studies in Construction Materials*, *16*, e00824. https://doi.org/10.1016/j.cscm.2021.e00824

Manalo, A., Sirimanna, C., Karunasena, W., McGarva, L., & Falzon, P. (2016). Pre-impregnated carbon fibre reinforced composite system for patch repair of steel I-beams. *Construction and Building Materials*, *105*, 365–376. https://doi.org/10.1016/j.conbuildmat.2015.12.172.

Martinelli, L., & Domaneschi, M. (2017). Effect of structural control on wind fatigue mitigation in suspension bridges. International Journal of Structural Engineering, 8(4), 289–307.

Mohammed, A. A., Manalo, A. C., Ferdous, W., Zhuge, Y., Vijay, P. V., Alkinani, A. Q., & Fam, A. (2020). State-of-the-art of prefabricated FRP composite jackets for structural repair. *Engineering Science and Technology, an International Journal*, *23*(5), 1244–1258. https://doi.org/10.1016/j.jestch.2020.02.006

Nazri, F. M. (2015). *Prediction of The Collapse Load for Moment-Resisting Steel Frame Structure Under Earthquake Forces (Penerbit USM)*. Penerbit USM.

Ngamkhanong, C., Kaewunruen, S., & Baniotopoulos, C. (2018). Far-Field Earthquake responses of overhead line equipment (OHLE) structure considering soil-structure interaction. *Frontiers in Built Environment*, *4*, 35.

Photiou, N. K., Hollaway, L. C., & Chryssanthopoulos, M. K. (2006). *Strengthening of an artificially degraded steel beam utilising a carbon / glass composite system*. *20*, 11–21. https://doi.org/10.1016/j.conbuildmat.2005.06.043

Seica, M. V., & Packer, J. A. (2007). FRP materials for the rehabilitation of tubular steel structures, for underwater applications. *Composite Structures*, *80*(3), 440–450. https://doi.org/10.1016/j.compstruct.2006.05.029

Siddique, M. A. A., & El Damatty, A. A. (2013). Improvement of local buckling behaviour of steel beams through bonding GFRP plates. *Composite Structures*, *96*, 44–56. https://doi.org/10.1016/j.compstruct.2012.08.042

Siwowski, T. W., & Siwowska, P. (2018). Experimental study on CFRP-strengthened steel beams. *Composites Part B: Engineering*, *149*(April), 12–21.

Tafsirojjaman, T., Fawzia, S., & Thambiratnam, D. (2019a). Enhancement Of Seismic Performance Of Steel Frame Through CFRP Strengthening. *Procedia Manufacturing*, *30*, 239–246. https://doi.org/10.1016/j.promfg.2019.02.035

Tafsirojjaman, T., Fawzia, S., & Thambiratnam, D. (2019b). Numerical investigation on the seismic strengthening of steel frame by using normal and high modulus CFRP. *Proceedings of the Seventh Asia-Pacific Conference on FRP in Structures (APFIS2019)*.

Tafsirojjaman, T., Fawzia, S., & Thambiratnam, D. (2020a). Numerical investigation on the cfrp strengthened steel frame under earthquake. *Materials Science Forum*, *995*, 123–129. https://doi.org/10.4028/www.scientific.net/MSF.995.123

Tafsirojjaman, T., Fawzia, S., & Thambiratnam, D. P. (2020b). Investigation on the behaviour of CFRP strengthened CHS members under Monotonic loading through finite element modelling. *Structures*, *28*, 297–308. https://doi.org/10.1016/j.istruc.2020.08.059

Tafsirojjaman, T., Fawzia, S., & Thambiratnam, D. P. (2021). Structural behaviour of CFRP strengthened beam-column connections under monotonic and cyclic loading. *Structures*, *33*(May), 2689–2699. https://doi.org/10.1016/j.istruc.2021.06.028

Tafsirojjaman, T., Fawzia, S., Thambiratnam, D. P., & Wirth, N. (2021). Performance of FRP strengthened full-scale simply-supported circular hollow steel members under monotonic and large-displacement cyclic loading. *Engineering Structures*, *242*(December 2020), 112522. https://doi.org/10.1016/j.engstruct.2021.112522

Tafsirojjaman, T., Fawzia, S., Thambiratnam, D. P., & Zhao, X. L. (2020a). Study on the cyclic bending behaviour of CFRP strengthened full-scale CHS members. *Structures*, *28*, 741–756. https://doi.org/10.1016/j.istruc.2020.09.015

Tafsirojjaman, T., Fawzia, S., Thambiratnam, D., & Zhao, X. (2020b). Numerical investigation of CFRP strengthened RHS members under cyclic loading. *Structures*, *24*, 610–626. https://doi.org/10.1016/j.istruc.2020.01.041

Tafsirojjaman, T., Fawzia, S., Thambiratnam, D., & Zhao, X. L. (2019a). Behaviour of CFRP strengthened CHS members under monotonic and cyclic loading. *Composite Structures*, *220*, 592–601. https://doi.org/10.1016/j.compstruct.2019.04.029

Tafsirojjaman, T., Fawzia, S., Thambiratnam, D., & Zhao, X. L. (2019b). Seismic strengthening of rigid steel frame with CFRP. *Archives of Civil and Mechanical Engineering*, *19*(2), 334–347. https://doi.org/10.1016/j.acme.2018.08.007

Tafsirojjaman, T., Fawzia, S., Thambiratnam, D., & Zhao, X. L. (2021). FRP strengthened SHS beam-column connection under monotonic and large-deformation cyclic loading. *Thin-Walled Structures*, *161*, 107518. https://doi.org/10.1016/j.tws.2021.107518

Zhao, X. L., Fernando, D., & Al-Mahaidi, R. (2006). CFRP strengthened RHS subjected to transverse end bearing force. *Engineering Structures*, *28*(11), 1555–1565. https://doi.org/10.1016/j.engstruct.2006.02.008

Zhao, X. L., & Zhang, L. (2007). State-of-the-art review on FRP strengthened steel structures. *Engineering Structures*, *29*(8), 1808–1823. https://doi.org/10.1016/j.engstruct.2006.10.006

Zhou, H., Fernando, D., Chen, G., & Kitipornchai, S. (2017). The quasi-static cyclic behaviour of CFRP-to-concrete bonded joints: An experimental study and a damage plasticity model. *Engineering Structures*, *153*, 43–56. https://doi.org/10.1016/j.engstruct.2017.10.007

Zhu, K., Al-Bermani, F. G. A., Kitipornchai, S., & Li, B. (1995). Dynamic response of flexibly jointed frames. *Engineering Structures*, *17*(8), 575–580. https://doi.org/10.1016/0141-0296(95)00008-U